Plasmonics (2021) 16:83–90
https://doi.org/10.1007/s11468-020-01260-1

Ultra-broadband Near-Unity Light Absorption by Disjunct Scattering Resonances of Disordered Nanounits Created with Atomic Scale Shadowing Effect

Imre Ozbay [1] · Amir Ghobadi [1,2] · Ekmel Ozbay [1,2,3,4,5]

Received: 8 June 2020 / Accepted: 9 August 2020 / Published online: 20 August 2020

Abstract
Metamaterial perfect absorbers have been the subject of many studies in recent years. Near-unity light harvesting in an ultra-broadband frequency range is the prime goal in many applications such as photoconversion systems. While the most common designs for achieving this goal are periodic plasmonic architectures, this work reveals the unprecedented potential of random designs for ultra-broadband light absorption. A metal-insulator-metal (MIM) structure with a periodically patterned top layer has discrete translational symmetry. The proposed theory, supported by numerical simulations, unveils the fact that breaking this symmetry in the top layer introduces multiple resonant units with separate spectra, and the superposition of these separate resonances broaden the overall response. The random absorber is realized using the oblique angle deposition-induced atomic scale shadowing effect. Based on the experimental results and numerical calculations, the proposed disorder plasmonic design can propose unity absorption (> 90%) over the spectral range from 520 to 1270 nm.

Keywords Plasmonics · Fabry-Perot cavity · Metamaterial perfect absorber · Oblique angle deposition

Introduction

The interaction of an electromagnetic (EM) wave and material, or the so-called light-matter interaction, at the nano- and micrometer scales, is the operation essence of many (nano)photonics, (nano)optics, and optoelectronic devices [1–4]. While semiconductors, as essential building blocks of modern technology, mostly support electronic transitions in the ultraviolet (UV), visible, and short near-infrared (NIR) wavelengths, metals, if designed properly, can exhibit strong light-matter interaction throughout the entire EM spectrum [5]. The collective oscillation of conduction electrons, or so-called localized surface plasmon resonances (LSPRs), and inter-band transitions is the main responsible mechanism for light absorption in nanometals. The large wave vectors of surface plasmons trigger the confinement of EM fields into plasmonic islands (i.e., nanotanennas) with dimensions much smaller than the wavelength, and these local hot spots provide the opportunity to manipulate light below the diffraction limits.

The most frequently employed tool for the fabrication of such plasmonic nanoantennas is electron beam lithography (EBL). It has been experimentally demonstrated in various studies [6–9] that broadband metamaterial absorbers with metal-insulator-metal (MIM) structures with a patterned top metal layer can attain very high performance in terms of absorption bandwidth. However, it should be noted that EBL is essentially a high-cost and large-scale incompatible route. Furthermore, one of the main findings of the experiments involving EBL patterning tends to perform marginally better in experimental results compared with the simulations in terms of the overall absorption bandwidth. This was attributed to the introduction of fabrication imperfections. Imperfections in the fabrication routine tend to increase the variance of the

✉ Imre Ozbay
ozbayimre@gmail.com

✉ Ekmel Ozbay
ozbay@bilkent.edu.tr

[1] NANOTAM–Nanotechnology Research Center, Bilkent University, 06800 Ankara, Turkey

[2] Department of Electrical and Electronics Engineering, Bilkent University, 06800 Ankara, Turkey

[3] UNAM–National Nanotechnology Research Center, Bilkent University, 06800 Ankara, Turkey

[4] Institute of Materials Science and Nanotechnology, Bilkent University, 06800 Ankara, Turkey

[5] Department of Physics, Bilkent University, 06800 Ankara, Turkey

periodic structure, making them sort of aperiodic. In other words, breaking of the translational symmetry on a small scale introduces an improvement in the overall absorptive bandwidth. This raises the question: How much more symmetry breaking can cause better overall absorption? In this study, we try to answer this question and understand the mechanism underlying this effect.

Although nanoimprint lithography (NIL) can be used to pattern nanounits in large areas, this tool is also high cost and complex, and the fabrication of tightly packed, high aspect ratio nanodesigns is generally challenging. To tackle this bottleneck, lithography-free approaches can be adopted to obtain nanostructured designs. On the other hand, recent reports have shown that disordered and aperiodic designs can outperform periodic designs due to the excitation of spectrally broad adjacent resonant modes [10–13]. Therefore, several lithography-free designs were fabricated recently to achieve near-unity light absorption in dimensions much smaller than the wavelength [6, 8, 14–41]. The strong light-matter interaction in this lithography-free planar design can be acquired through the strong interference in planar ultrathin designs [42–45]. However, a substantial enhancement in light absorption capability of a metamaterial design could be achieved via surface texturing. The most common approach is to use trapping wavelength-scale nanostructured scaffolds to harvest the incoming light. However, these designs are essentially bulky, and their fabrication route has material restriction. Dewetting-induced surface texturing [31], nanohole [32], and nanoparticle formation [46] are some of innovative approaches to obtain nanounits in ultrathin dimensions. Laser-induced deformation [47–50] and tuning the deposition conditions [51] are some other examples for the formation of nanostructures in ultrathin geometries. However, these methods have two main bottlenecks: (1) they need large thermal budgets, and this could cause deficiencies in the material properties, and (2) similar to other bottom up approaches, they have material imitations. Moreover, these methods are efficient only in ultrathin dimensions, and they lose their functionality in thick layers.

Oblique angle deposition is an alternative approach to realize two-/three-dimensional (2D/3D) nanostructures with no material restriction [52]. Unlike dewetting, this process can be adopted for any material with any layer thickness; thus, it can be used to achieve high aspect ratio 3D nanostructures. Moreover, this process is done in room temperature that can be potentially used to fabricate flexible absorber platforms. In this approach, a sample is placed in a position that is oblique to evaporated atoms. When the flux reaches the substrate, an additional factor is introduced into the growth process, which can result in nanostructures instead of a continuous layer. It is generally accepted that the mechanistic factor controlling the nanostructural evolution of the films is an atomic scale "shadowing effect," which prevents the deposition of particles in regions situated behind initially formed nuclei (i.e., shadowed regions). We have successfully adopted this approach for the design of 3D ultra-broadband absorbers in visible, near-infrared (NIR) [53–55] and mid-infrared (MIR) [56, 57] light-harvesting devices. Taking all into consideration, the oblique angle deposition, with its random geometry and capability to synthesize nanostructures with no material restriction, is an excellent approach to realize high-performance perfect absorbers in large-scale dimensions.

In this work, we adopt this technique to achieve ultra-broadband light absorption in a simple MIM structure. According to the presented study, the shadowing effect due to oblique angle deposition introduces the following effects that break the symmetry of the deposited top metal layer of an MIM structure: (i) nanoislands are spaced randomly, (ii) nanoislands have lateral sizes variation, and (iii) nanoislands have significant height variation. In this manner, separate resonances are induced for varying nanoisland sizes. Each island acts as a separate scatterer, and each scatterer is active within its own resonant spectrum and effective scattering cross section. Our numerical analysis reveals that the spacing between random nanoislands has great importance for absorber performance. As long as the scattering cross section of each scatterer encompasses an area with multiple islands inside, then a broad range of wavelengths can be harvested. According to our characterization findings, an absorption above 0.9 is achieved in a range spanning from 520 to 1270 nm. The mechanisms responsible for this light-harvesting response are discussed in detail.

Results and Discussion

Disordered structures can provide excellent light-harvesting capabilities. In order to conduct numerical work on this idea, you can construct very large simulation domains and try to design a non-periodic random structure manually. In such a system, one would need various geometries and random placement of each geometry. This work would, however, be quite tedious and not worthwhile since the randomness will be determined by the experimental conditions and not by design. Therefore, one would rather resort to more practical approaches. Since the impact of each geometry on the overall absorption performance of the cavity must be known, the power of periodic simulations can be used, and the inclination of absorption spectra can be observed as the unit cell is modified. For this purpose, firstly periodic unit cells are used. This way, we can understand the required distribution of random geometries for broadband absorption. To have a simplified picture, the top plasmonic nanounits have been chosen as a disc. In our simplified model, three main geometrical properties define the absorption wavelengths and bandwidth of the design: (i) insulator thickness (D_I), (ii) top nanodisc metal

thickness (D_M), and (iii) nanodisc radius (R). Figure 1a represents the contour plot of the absorption profile with respect to the insulator layer thickness. As clearly shown in this figure, a single resonance mode exists for thin insulator thicknesses, but a second resonance emerges as we move to thicker layers. For D_I above 60 nm, both of these modes experience a gradual red shift. However, it should be noted that the effect of insulator thickness is relatively limited as shown in the experimental section; similar results were obtained for $D_I = 70$ nm and $D_I = 90$ nm. A different story can be found for D_M (see Fig. 1b); a double-resonance response is observed. While one of these resonances weakly depends on the disc geometry, the other mode undergoes a strong blue-shift for increasing the disc height, D_M. Finally, as seen in Fig. 1c, again, a double-resonance response is observed with one resonance weakly depending on the disc radius and the other mode undergoing strong redshift for increasing disc radius, R. Therefore, essentially, tuning the geometries of the disc can be used as a means to tailor the absorption response of the cavity. Hypothetically, a hybrid structure consisting of multi-dimensional/shape nanounits could cover a broad wavelength regime compared with a single periodic design. However, the question here is can we consider these nanounits as isolated resonators such that the existence of multiple resonance modes leads to an overall near-unity broadband absorption. To find an answer to this question, we build a unit cell as shown in Fig. 1d. In this unit cell, one of the components is held at a fixed position, and the other one gradually moves away from the first in order to identify the required gap distance for isolated behavior. As plotted in Fig. 1f, at close proximity of nanodiscs, a double-resonance behavior is probed, but increasing the gap distance causes one of the modes to disappear and the other mode to have a broadened spectrum. Thus, intuitively, one of these resonances originates

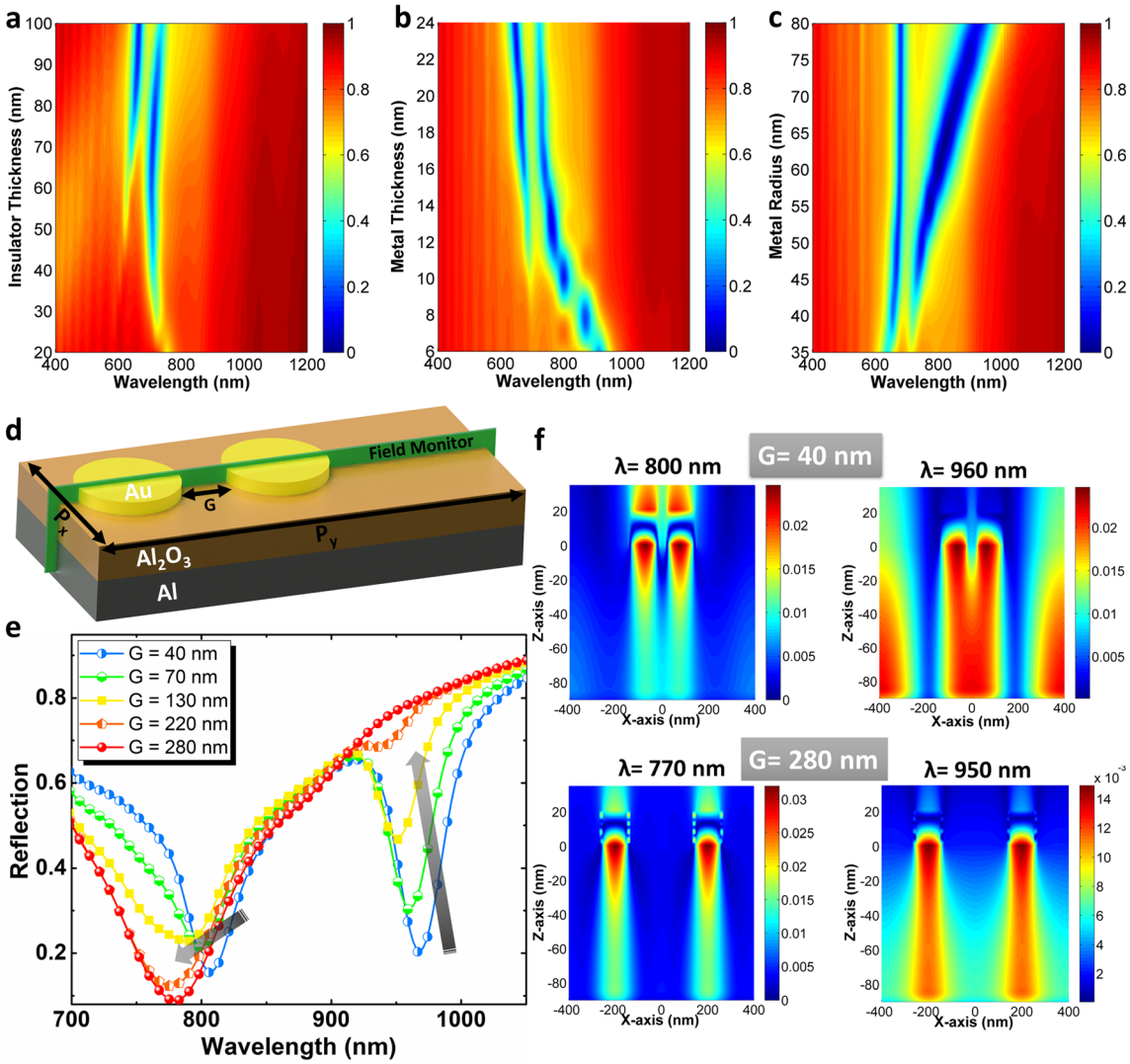

Fig. 1 **a** Reflection spectra for insulator thickness (D_I) sweep. **b** Reflection spectra for top metal thickness (D_M) sweep. **c** Reflection spectra for top metal radius (R) sweep. **d** Unit cell with two nanodiscs with lateral spacing distance (G). **e** Reflection spectral for changing spacing distance (G). **f** H-field distribution for $G = 40$ nm and $G = 280$ nm

from the lateral cavity formed between two adjacent discs. Coupling between these discs causes a resonance that very strongly depends on the gap distance, and this coupling loses its strength approximately after the gap distance exceeds the nanodisc diameter. The other mode is independent of the gap distance and essentially belongs to a single isolated nanoresonator. The broadening of the spectrum with increasing gap originates from the fact that the absorbers are more uniformly distributed on the simulation domain when they are further apart. In terms of a soccer analogy, if you can place multiple goalkeepers in front of the same goal, you would like to have them uniformly spaced in order to have the best chances of catching the ball.

To have a better comparison, we have compared the magnetic field (H-field) profiles across the cavity for two different gap distances (G) of 4 nm and 280 nm (see Fig. 1f). For the case of $G = 40$ nm, at the lowest wavelength resonance of 800 nm, the magnetic field is dominantly localized underneath the nanodiscs. However, the longer wavelength resonance, 960 nm, has led to the field localization in both below and between nanodiscs. Therefore, the first resonance mode is a localized surface plasmon resonance (LSPR), while the second mode is propagating surface plasmons (PSPs) in the continuous bottom metal film. Previous studies have reported that the addition of a flat layer (to form MIM cavity) can trigger the excitation of PSPs in bottom metal-insulator interface [9, 58–60]. In other words, in small gap distances, the adjacent two elements perform as a single effective element that can excite PSP resonances. For the separated disc configuration, the H-field shows the same profile in both on and off resonance wavelengths, and it is essentially LSPR modes confined beneath the nanoantennas. We observed that further increasing the gap distance beyond 200 nm caused little change in the field profile shape around the nanodiscs.

Gaining an insight on the impact of geometrical dimensions on the absorption response of the MIM cavity, the shape of elements, as an important factor, should be scrutinized. For this purpose, four common shapes of disc, rectangle, rhomboid, and ring have been chosen (see Fig. 2a). Shapes are selected to represent the richness in the surface morphology of the resultant layer, obtained from SEM image analysis. The circle models the common semi-spherical nanoislands, the rectangle represents elongated nanoislands, rhomboid shows the impact of sharp corners in the textured film, and ring is to model the nanoholes formed within the layer. As illustrated in Fig. 2b, this design shows four resonance modes across the simulation spectrum. To identify the nature of these resonance frequencies, the H-filed field distribution in a lateral plane (in the top metal-spacer interface) is extracted. As shown in Fig. 2c, at each resonance frequency, only the corresponding one of the four plasmonic elements is active. Therefore, we conclude that the resonances are disjunct/disjoint. The superposition of the spectral absorbance of disjunct resonances has led to an ultra-broadband light absorption. Therefore, from all the above discussions, a random design with multi-dimensions, multi-spacing, and multi-shapes could be an ideal design for ultra-broadband light absorption.

To realize this disordered design, oblique angle deposition is utilized at ~ 80^0 incidence angle. Angles below this value reduce the shadowing effect, and rather than formation of nanoparticles,

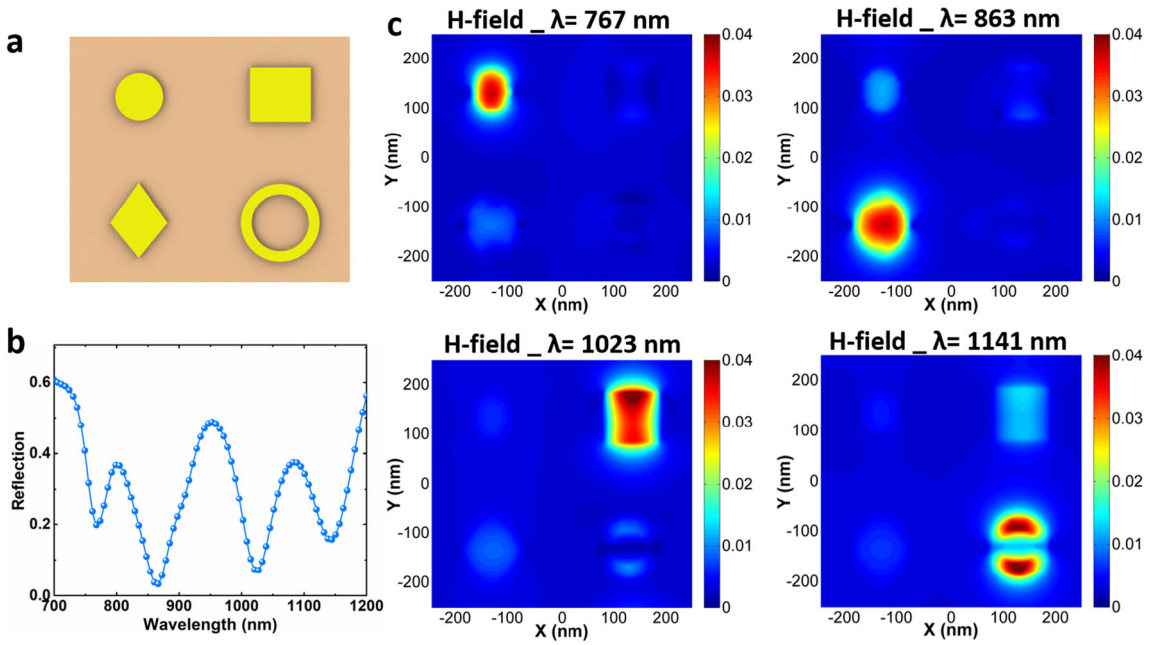

Fig. 2 **a** Schematic of the system with four nanoisland geometries: circle, rectangle, rhomboid, and ring. **b** The reflection spectrum of the given system around the absorption wavelengths. **c** The H-field distribution beneath the top layer (the top metal and dielectric spacer interface) for the corresponding reflection dips located at $\lambda = 767$ nm, $\lambda = 863$ nm, $\lambda = 1023$ nm, and $\lambda = 1141$ nm

continuous films are made. In the other end of the limit, i. e., angles above 80^0, the shadowing effect becomes dominant, and consequently, the nanoparticle spacing significantly grows. Thus, the gold filling fraction reduces, and absorption response loses its strength. In 80^0, we have both nanoparticle formation and large particle density to achieve the strongest absorption response. The details have been given in the experimental section. Briefly, the bottom optically thick (100 nm) aluminum (Al) layer is coated with thermal evaporation. Later, the sample is transferred into an atomic layer deposition (ALD) chamber to coat the spacer aluminum dioxide (Al_2O_3) layer. The spacer layer thicknesses (D_I) are chosen as 70 nm and 90 nm. Finally, oblique angle deposition is adopted to achieve the random top nanounits by the evaporation of Au source. The nominal thickness of the islands is set as 14 nm.

Figure 3a depicts the cross-sectional scanning electron microscope (SEM) images of the MIM cavity. The figure shows the uniform growth of all three layers. To have a clearer picture of the morphology of the top nanoislands, side and top view images are also obtained, as shown in Fig. 3a. As these panels reveal the top layer morphology has variability in multiple dimensions including shape of nanoislands and inter island spacing, atomic force microscopy (AFM) results in Fig. 3b also verify this fact that the randomness of the units is not only on their lateral dimensions but also on their thicknesses. Upon the structural characterization of the cavity designs, their optical performance is studied. Figure 3c illustrates the absorption response of the cavities with two different D_Is of 70 nm and 90 nm. As this graph shows, both designs have an ultra-broadband absorption response. For the case of D_I = 70 nm, the absorption bandwidth covers a range spanning from 440 to 995 nm, while the thicker spacer layer provides near-unity absorption (above 0.9) from 450 to 1250 nm. The insulator thickness has two main effects, as shown in Fig. 1a: (i) it slightly redshifts the resonance wavelength, and (ii) as the insulator layer thickness increases, a new resonance mode appears. Thus, moving from 70 to 90 nm, the absorption edges (both lower and upper

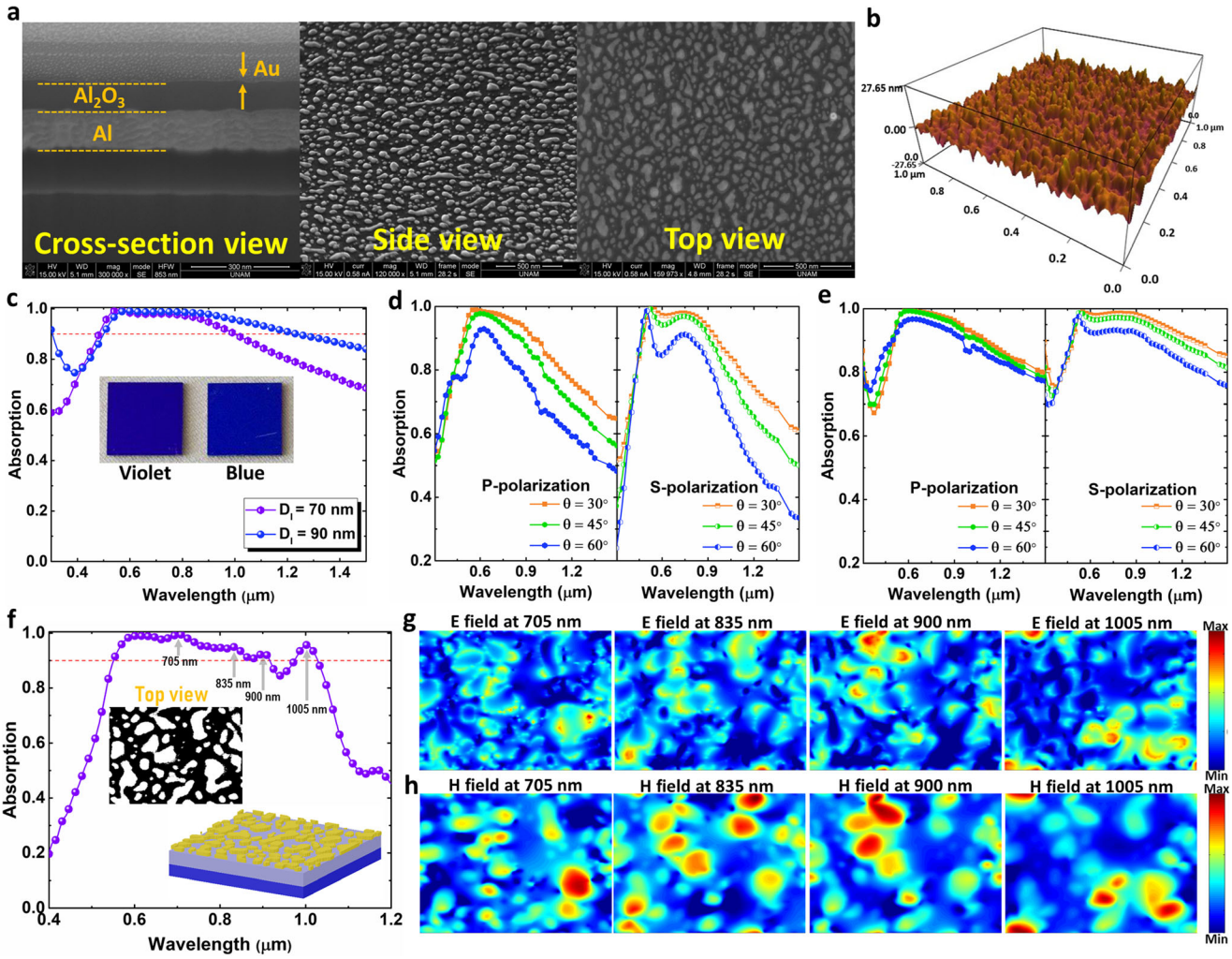

Fig 3 **a** The cross section, side, and top view SEM images of the fabricated sample. **b** AFM image of the top surface. **c** The absorption spectra of the fabricated samples with two different spacer thicknesses, the angular response of the MIM samples with (**d**) D_I = 70 nm, and (**e**) D_I = 90 nm for both p and s polarizations. **f** The simulated absorption spectra, **g** E-field, and **h** H-field distributions at the top metal plane for the random design

ones) are red-shifted, and this can be seen from Fig. 3c. Moreover, the double-resonance feature in thicker layers makes the overall absorption more close to unity with a broader bandwidth. The angular response of the design has also been studied in both p and s polarizations, for three different incidence angles of 30°, 45°, and 60°. As exhibited in Fig. 3d–e, the cavity retains its absorption high in all incoming angles and polarizations. To analyze this broad absorption response numerically, through using the obtained SEM images, a realistic simulation file was constructed with multiple scatterers of various geometries. Using a home-made algorithm, the fill fraction of the nanoislands from the top SEM image was determined, and particles were classified into size groups as (i) very small, fitting in a disc of 10 nm radius; (ii) small, fitting in a disc of 18 nm radius; (iii) medium, fitting in a disc of 32 nm radius; and (iv) large, not fitting in a disc of 32 nm radius. Nanoislands within the same size group were extracted as a separate image file. A total of 4 image files were generated each corresponding to a different size group. Each size group was assigned a separate thickness value of (i) 7 nm, (ii) 10 nm, (iii) 15 nm, and (iv) 22 nm, respectively, and imported to Lumerical FDTD Solutions with the corresponding thickness value. Calculations were carried out such that the total gold mass would be equal to the total deposited mass in the thermal evaporator. In the end, we obtained a numerical model that had multiple shapes of multiple sizes, geometries, and various thicknesses. Simulation result shown in Fig. 3f shows very good agreement with the experiment. A close look at the field distribution given in Fig. 3g and h shows that, at different reflection dips, different regions are "active." Therefore, this demonstrates the fact that separate wavelengths are absorbed at separate centers. These centers can be composed of a single island or a closely spaced coupled island ensemble. Electromagnetic waves are not absorbed homogeneously and continuously but rather spatially localized islands or island ensembles. Furthermore, when the simulated incident light polarization is rotated (no figure provided), little change occurs in the absorption level. This is possibly due to the random structures' ability to absorb incident light independently. Overall, these results shed some light into the nature of the absorption of light by random plasmonic structures.

Conclusion

Taking all of the above-mentioned results into consideration, a random plasmonic design could lead to an ultra-broadband light near perfect absorption. In light of the numerical and experimental results that we provided so far, nanoislands whose separation with the nearest neighbor exceeds its own size can be treated as standalone nanoislands. Such standalone nanoislands will absorb a bandwidth determined solely by their own electromagnetic response, and these plasmonic islands will capture their effective resonant spectrum within a range of their characteristic capture cross section (scattering cross section). Islands with larger dimensions tend to have multi-resonant spectra, thus covering a larger band. On the other hand, coupled islands with a nearest neighbor closer than their own size will have multi-resonant spectra. These multi-resonant spectra occurring from standalone islands and coupled islands will contribute to the overall absorption by absorbing a wider spectral band. All of the aforementioned effects contribute to greater than 99% absorption in the spectral range 550–950 nm and in overall greater than 90% absorption in a broad range from 520 to 1270 nm.

Experimental Section

Device fabrication

For the fabrication of this cavity design, in the first step, the Si substrate has been diced into 1 cm*1 cm pieces. Afterward, these substrates are placed inside a Piranha solution, followed by hydrofluoric (HF) to remove the organic and unwanted metal oxide layer. To coat Al and Au layers, thermal evaporator machine is employed. The deposition rate is fixed at 3 A°/sec for both layers, and the chamber pressure is brought down into 5e-6 Torr throughout the deposition process. The Al_2O_3 depositions were carried out at 200 °C in an ALD reactor (Cambridge Nanotech Savannah S100) employing $Al(CH_3)_3$ solution as the Al precursor and water as the oxygen source. The pulse and purge durations were set as 0.02 s and 15 s, respectively. The growth rate was found to be 1.01 A° per cycle. Finally, oblique angle deposition is utilized to achieve the random design. For this aim, the same procedure as ordinary thermal evaporation is utilized; only the sample is positioned oblique to the source (~ 80°).

Optical characterization

To measure the absorption of the design in normal illumination, in the range of 0.3–1.5 μm, we used an in-house setup. The setup uses a halogen lamp as the source, and this source is connected to a microscope to collect the data. This data is entered into a spectrometer (Newport OSM2). In all of the measurements, the obtained intensities are normalized with the reflection data from a thick Al-coated sample (which has near 100% reflection in our desired frequency range). Finally, a personal computer (PC) is utilized to extract and monitor the data. In addition, the angular response of the design is measured utilizing a spectroscopic ellipsometer tool (J. A. Woollam Co. Inc. V-VASE) at two different s and p polarizations. The angle of incidence is set as 30°, 45°, and 60°.

Funding Information Authors acknowledge financial support from DPT-HAMIT and TUBITAK projects under Nos. 113E331 and 109E301. One of the authors (E. O.) also acknowledges partial support from the Turkish Academy of Sciences.

References

1. Ji C, Lee KT, Xu T, Zhou J, Park HJ, Guo LJ (2017) Engineering Light at the Nanoscale: structural color filters and broadband perfect absorbers. Adv Opt Mater 5:1–22. https://doi.org/10.1002/adom.201700368
2. Ghobadi A, Hajian H, Butun B, Ozbay E (2018) Strong light-matter interaction in lithography-free planar metamaterial perfect absorbers. ACS Photonics 5:4203–4221. https://doi.org/10.1021/acsphotonics.8b00872
3. Hajian H, Ghobadi A, Butun B, Ozbay E (2019) Active metamaterial nearly perfect light absorbers: a review [Invited]. J Opt Soc Am B 36:F131. https://doi.org/10.1364/josab.36.00f131
4. Ghobadi A, Ulusoy Ghobadi TG, Karadas F, Ozbay E (2019) Semiconductor thin film based metasurfaces and metamaterials for photovoltaic and photoelectrochemical water splitting applications. Adv Opt Mater 7:1900028. https://doi.org/10.1002/adom.201900028
5. Ozbay E (2006) Plasmonics: merging photonics and electronics at nanoscale dimensions. Science 311(80):189–194. https://doi.org/10.1126/science.1114849
6. Li Z, Butun S, Aydin K (2015) Large-area, lithography-free super absorbers and color filters at visible frequencies using ultrathin metallic films. ACS Photonics 2:183–188. https://doi.org/10.1021/ph500410u
7. Ozbay I, Ghobadi A, Butun B, Turhan-Sayan G (2020) Bismuth plasmonics for extraordinary light absorption in deep subwavelength geometries. Opt Lett 45:686. https://doi.org/10.1364/ol.45.000686
8. Li Z, Palacios E, Butun S, Kocer H, Aydin K (2015) Omnidirectional, broadband light absorption using large-area, ultrathin lossy metallic film coatings. Sci Rep 5:1–22. https://doi.org/10.1038/srep15137
9. Ding F, Dai J, Chen Y, Zhu J, Jin Y, Bozhevolnyi SI (2016) Broadband near-infrared metamaterial absorbers utilizing highly lossy metals. Sci Rep 6:39445. https://doi.org/10.1038/srep39445
10. Battaglia C, Hsu CM, Söderström K, Escarré J, Haug FJ, Charrière M, Boccard M, Despeisse M, Alexander DTL, Cantoni M, Cui Y, Ballif C (2012) Light trapping in solar cells: can periodic beat random? ACS Nano 6:2790–2797. https://doi.org/10.1021/nn300287j
11. Dewan R, Shrestha S, Jovanov V, Hüpkes J, Bittkau K, Knipp D (2015) Random versus periodic: determining light trapping of randomly textured thin film solar cells by the superposition of periodic surface textures. Sol Energy Mater Sol Cells 143:183–189. https://doi.org/10.1016/j.solmat.2015.06.014
12. Pratesi F, Burresi M, Riboli F, Vynck K, Wiersma DS (2013) Disordered photonic structures for light harvesting in solar cells. Opt Express 21:A460. https://doi.org/10.1364/oe.21.00a460
13. Pala RA, Liu JSQ, Barnard ES, Askarov D, Garnett EC, Fan S, Brongersma ML (2013) Optimization of non-periodic plasmonic light-trapping layers for thin-film solar cells. Nat Commun 4:1–7. https://doi.org/10.1038/ncomms3095
14. Lee K-T, Jang J-Y, Park SJ, Ji C, Guo LJ, Park HJ (2016) Subwavelength nanocavity for flexible structural transmissive color generation with a wide viewing angle. Optica 3:1489–1495. https://doi.org/10.1364/OPTICA.3.001489
15. Li Z, Butun S, Aydin K (2016) Lithography-free transmission fi lters at ultraviolet frequencies using ultra-thin aluminum films. J Opt 18:065006. https://doi.org/10.1088/2040-8978/18/6/065006
16. Zhao Y, Zhao Y, Hu S, Lv J, Ying Y, Gervinskas G, Si G (2017) Artificial structural color pixels: a review. Materials (Basel) 10:944. https://doi.org/10.3390/ma10080944
17. Yoon Y-T, Lee S-S (2010) Transmission type color filter incorporating a silver film based etalon. Opt Express 18:5344–5349. https://doi.org/10.1364/OE.18.005344
18. Zhao D, Meng L, Gong H, Chen X, Chen Y, Yan M, Li Q, Qiu M (2014) Ultra-narrow-band light dissipation by a stack of lamellar silver and alumina. Appl Phys Lett 104:221107. https://doi.org/10.1063/1.4881267
19. Lee JY, Lee KT, Seo S, Guo LJ (2014) Decorative power generating panels creating angle insensitive transmissive colors. Sci Rep 4:4192. https://doi.org/10.1038/srep04192
20. Mirshafieyan SS, Gregory DA (2018) Electrically tunable perfect light absorbers as color filters and modulators. Sci Rep 8:1–9. https://doi.org/10.1038/s41598-018-20879-z
21. Eng HAOP, Uo YIL, Ing XIY et al (2016) Broadband and highly absorbing multilayer structure in mid-infrared. Appl Opt 55:8833–8838
22. Ghobadi A, Dereshgi SA, Butun B, Ozbay E (2017) Ultra-broadband asymmetric light transmission and absorption through the use of metal free multilayer capped dielectric microsphere resonator. Sci Rep 7:14538. https://doi.org/10.1038/s41598-017-15248-1
23. Mattiucci N, Bloemer MJ, Akozbek N, D'Aguanno G (2013) Impedance matched thin metamaterials make metals absorbing. Sci Rep 3:1–11. https://doi.org/10.1038/srep03203
24. Chirumamilla M, Roberts AS, Ding F, Wang D, Kristensen PK, Bozhevolnyi SI, Pedersen K (2016) Multilayer tungsten-alumina-based broadband light absorbers for high-temperature applications. Opt Mater Express 6:2704. https://doi.org/10.1364/OME.6.002704
25. Deng H, Li Z, Stan L, Rosenmann D, Czaplewski D, Gao J, Yang X (2015) Broadband perfect absorber based on one ultrathin layer of refractory metal. Opt Lett 40:2592–2595
26. Kajtár G, Kafesaki M, Economou EN, Soukoulis CM (2016) Theoretical model of homogeneous metal–insulator–metal perfect multi-band absorbers for the visible spectrum. J Phys D Appl Phys 49:055104. https://doi.org/10.1088/0022-3727/49/5/055104
27. Ding F, Mo L, Zhu J, He S (2015) Lithography-free, broadband, omnidirectional, and polarization-insensitive thin optical absorber. Appl Phys Lett 106:061108. https://doi.org/10.1063/1.4908182
28. Zhong YK, Lai Y-C, Tu M-H, Chen BR, Fu SM, Yu P, Lin A (2016) Omnidirectional, polarization-independent, ultra-broadband metamaterial perfect absorber using field-penetration and reflected-wave-cancellation. Opt Express 24:A832. https://doi.org/10.1364/OE.24.00A832
29. Zhong YK, Tu M, Chen B et al (2016) Fully planarized perfect metamaterial absorbers with no photonic nanostructures. IEEE Photonics J 8:2200109–2200109. https://doi.org/10.1109/JPHOT.2015.2507368
30. Fu SM, Zhong YK, Tu MH, Chen BR, Lin A (2016) A fully functionalized metamaterial perfect absorber with simple design and implementation. Sci Rep 6:36244. https://doi.org/10.1038/srep36244
31. Ghobadi A, Dereshgi SA, Hajian H, Bozok B, Butun B, Ozbay E (2017) Ultra-broadband , wide angle absorber utilizing metal insulator multilayers stack with a multi- thickness metal surface texture. Sci Rep 7:4755. https://doi.org/10.1038/s41598-017-04964-3
32. Ghobadi A, Hajian H, Dereshgi SA, Bozok B, Butun B, Ozbay E (2017) Disordered nanohole patterns in metal-insulator multilayer for ultra-broadband light absorption: atomic layer deposition for lithography free highly repeatable large scale multilayer growth. Sci Rep 7:1–10. https://doi.org/10.1038/s41598-017-15312-w
33. Ghobadi A, Hajian H, Gokbayrak M, Butun B, Ozbay E (2019) Bismuth-based metamaterials: from narrowband reflective color filter to extremely broadband near perfect absorber. Nanophotonics 8:823–832. https://doi.org/10.1515/nanoph-2018-0217
34. Soydan MC, Ghobadi A, Yildirim DU, Erturk VB, Ozbay E (2019) All ceramic-based metal-free ultra-broadband perfect absorber. Plasmonics 1:1–15. https://doi.org/10.1007/s11468-019-00976-z

35. Mao K, Shen W, Yang C, Fang X, Yuan W, Zhang Y, Liu X (2016) Angle insensitive color filters in transmission covering the visible region. Sci Rep 6:19289. https://doi.org/10.1038/srep19289
36. Park CS, Shrestha VR, Lee SS, Kim ES, Choi DY (2015) Omnidirectional color filters capitalizing on a nano-resonator of Ag-TiO2 -Ag integrated with a phase compensating dielectric overlay. Sci Rep 5:8467. https://doi.org/10.1038/srep08467
37. Lee K-T, Seo S, Lee JY, Guo LJ (2014) Strong resonance effect in a lossy medium-based optical cavity for angle robust spectrum filters. Adv Mater 26:6324–6328. https://doi.org/10.1002/adma.201402117
38. Han JH, Kim D-Y, Kim D, Choi KC (2016) Highly conductive and flexible color filter electrode using multilayer film structure. Sci Rep 6:29341. https://doi.org/10.1038/srep29341
39. Lee KT, Seo S, Yong Lee J, Jay Guo L (2014) Ultrathin metal-semiconductor-metal resonator for angle invariant visible band transmission filters. Appl Phys Lett 104:231112. https://doi.org/10.1063/1.4883494
40. Yang C, Shen W, Zhang Y, Li K, Fang X, Zhang X, Liu X (2015) Compact multilayer film structure for angle insensitive color filtering. Sci Rep 5:9285. https://doi.org/10.1038/srep09285
41. Lee KT, Han SY, Park HJ (2017) Omnidirectional flexible transmissive structural colors with high-color-purity and high-efficiency exploiting multicavity resonances. Adv Opt Mater 5:1700284. https://doi.org/10.1002/adom.201700284
42. Ghobadi A, Hajian H, Soydan MC, Butun B, Ozbay E (2019) Lithography-free planar band-pass reflective color filter using series connection of cavities. Sci Rep 9:1–11. https://doi.org/10.1038/s41598-018-36540-8
43. Abedini Dereshgi S, Ghobadi A, Hajian H, Butun B, Ozbay E (2017) Ultra-broadband, lithography-free, and large-scale compatible perfect absorbers: the optimum choice of metal layers in metal-insulator multilayer stacks. Sci Rep 7:14872. https://doi.org/10.1038/s41598-017-13837-8
44. Hajian H, Ghobadi A, Butun B, Ozbay E (2017) Nearly perfect resonant absorption and coherent thermal emission by hBN-based photonic crystals. Opt Express 25:31970–31987. https://doi.org/10.1364/OE.25.031970
45. Ghobadi A, Demirag Y, Hajian H, Toprak A, Butun B, Ozbay E (2019) Spectrally selective ultrathin photodetectors using strong interference in nanocavity design. IEEE Electron Device Lett 40:1–928. https://doi.org/10.1109/led.2019.2910064
46. Ghobadi A, Hajian H, Rashed AR, Butun B, Ozbay E (2018) Tuning the metal filling fraction in metal-insulator-metal ultra-broadband perfect absorbers to maximize the absorption bandwidth. Photonics Res 6:168–176. https://doi.org/10.1364/PRJ.6.000168
47. Garrelie F, Colombier J-P, Pigeon F, Tonchev S, Faure N, Bounhalli M, Reynaud S, Parriaux O (2011) Evidence of surface plasmon resonance in ultrafast laser-induced ripples. Opt Express 19:9035. https://doi.org/10.1364/oe.19.009035
48. Han W, Jiang L, Li X, Wang Q, Wang S, Hu J, Lu Y (2017) Controllable plasmonic nanostructures induced by dual-wavelength femtosecond laser irradiation. Sci Rep 7:1–11. https://doi.org/10.1038/s41598-017-16374-6
49. Tseng ML, Chang CM, Chen BH, Huang YW, Chu CH, Chung KS, Liu YJ, Tsai HG, Chu NN, Huang DW, Chiang HP, Tsai DP (2012) Fabrication of plasmonic devices using femtosecond laser-induced forward transfer technique. Nanotechnology 23. https://doi.org/10.1088/0957-4484/23/44/444013
50. Li C, Hu J, Jiang L, Xu C, Li X, Gao Y, Qu L (2020) Shaped femtosecond laser induced photoreduction for highly controllable Au nanoparticles based on localized field enhancement and their SERS applications. Nanophotonics 9:691–702. https://doi.org/10.1515/nanoph-2019-0460
51. Liu Z, Liu X, Huang S, Pan P, Chen J, Liu G, Gu G (2015) Automatically acquired broadband plasmonic-metamaterial black absorber during the metallic film-formation. ACS Appl Mater Interfaces 7:4962–4968. https://doi.org/10.1021/acsami.5b00056
52. Grüner C, Liedtke S, Bauer J, Mayr SG, Rauschenbach B (2018) Morphology of thin films formed by oblique physical vapor deposition. ACS Appl Nano Mater 1:1370–1376. https://doi.org/10.1021/acsanm.8b00124
53. Soydan MC, Ghobadi A, Yildirim DU et al (2019) Lithography-free random bismuth nanostructures for full solar spectrum harvesting and mid-infrared sensing. Adv Opt Mater n/a:1901203. https://doi.org/10.1002/adom.201901203
54. Ghobadi TGU, Ghobadi A, Soydan MC, Vishlaghi MB, Kaya S, Karadas F, Ozbay E (2020) Strong light–matter interactions in Au plasmonic nanoantennas coupled with prussian blue catalyst on BiVO4 for photoelectrochemical water splitting. ChemSusChem 13:2577–2588. https://doi.org/10.1002/cssc.202000294
55. Ulusoy Ghobadi TG, Ghobadi A, Karadas F, Ozbay E (2020) Large scale compatible fabrication of gold capped titanium dioxide nanoantennas using a shadowing effect for photoelectrochemical water splitting. Int J Hydrog Energy 45:1521–1531. https://doi.org/10.1016/j.ijhydene.2019.11.060
56. Yildirim DU, Ghobadi A, Soydan MC, Atesal O, Toprak A, Caliskan MD, Ozbay E (2019) Disordered and densely packed ITO nanorods as an excellent lithography-free optical solar reflector metasurface. ACS Photonics 6:1812–1822. https://doi.org/10.1021/acsphotonics.9b00636
57. Soydan MC, Ghobadi A, Yildirim DU, Erturk VB, Ozbay E (2020) Deep subwavelength light confinement in disordered bismuth nanorods as a linearly thermal-tunable metamaterial. Phys Status Solidi Rapid Res Lett 2000066:1–6. https://doi.org/10.1002/pssr.202000066
58. Stuart HR, Hall DG (1998) Enhanced dipole-dipole interaction between elementary radiators near a surface. Phys Rev Lett 80:5663–5666. https://doi.org/10.1002/pola.23473
59. Cesario J, Quidant R, Badenes G, Enoch S (2005) Electromagnetic coupling between a metal nanoparticle grating and a metallic surface. Opt Lett 30:3404. https://doi.org/10.1364/ol.30.003404
60. Chu Y, Crozier KB (2009) Experimental study of the interaction between localized and propagating surface plasmons. Opt Lett 34:244. https://doi.org/10.1364/ol.34.000244